Available on the CERN CDS information server **CMS PAS SUS-12-024**

CMS Physics Analysis Summary

Contact: cms-pag-conveners-susy@cern.ch 2013/03/05

Search for gluino-mediated bottom- and top-squark production in pp collisions at 8 TeV

The CMS Collaboration

Abstract

A search for supersymmetry is presented based on events with large missing transverse energy, no isolated electron or muon, and at least three jets, at least one of which must be identified as a bottom-quark jet. A simultaneous examination of the number of events in exclusive bins of H_{T}, missing transverse energy, and bottom-quark jet multiplicity is performed, where H_{T} is the scalar sum of jet transverse momentum values. The sample consists of an integrated luminosity of 19.4 fb^{-1} of proton-proton collision data recorded at a center-of-mass energy of 8 TeV with the CMS detector at the LHC in 2012. The observed number of events is found to be consistent with the expectation from the standard model, which is evaluated with control samples in the data. The results are interpreted in the context of simplified models of new physics processes in which gluino pair production is followed by the decay of each gluino to an undetected particle and either two bottom quarks or two top quarks.

1 Introduction

The standard model (SM) of particle physics has proved to be remarkably successful in describing phenomena up to the highest energy scales that have been probed. Nonetheless, the SM is widely viewed to be incomplete. Many extensions have been proposed to provide a more fundamental theory. Supersymmetry (SUSY) [1–8], one such extension, postulates that each SM particle is paired with a SUSY partner from which it differs in spin by one-half unit, with otherwise identical quantum numbers. For example, squarks and gluinos are the SUSY partners of quarks and gluons, respectively. One of the principal motivations for SUSY is to stabilize the calculation of the Higgs boson mass. For this stabilization to be "natural" [9–11], top squarks, bottom squarks, and to a lesser extent gluinos, must be relatively light. If top and bottom squarks are light, their production is enhanced, either through direct pair production or through production mediated by gluinos, where the latter process is favored if the gluino production cross section is large. Since both top and bottom squarks decay to bottom quarks (the top squark through the top quark), natural SUSY models are characterized by an abundance of bottom-quark jets (b jets).

In R-parity-conserving [12] SUSY models, supersymmetric particles are created in pairs. Each member of the pair initiates a decay chain that terminates with the lightest SUSY particle (LSP) and SM particles, typically including jets. If the LSP only interacts weakly, as in the case of a dark-matter candidate, it escapes detection, potentially yielding significant missing transverse energy ($E_{\mathrm{T}}^{\mathrm{miss}}$). Thus large values of $E_{\mathrm{T}}^{\mathrm{miss}}$ provide another possible SUSY signature.

In this note, we present a search for SUSY in events with at least three jets, at least one tagged b jet, and large $E_{\mathrm{T}}^{\mathrm{miss}}$. The search is based on a sample of proton-proton collision data collected at $\sqrt{s} = 8\,\mathrm{TeV}$ with the Compact Muon Solenoid (CMS) detector at the CERN Large Hadron Collider (LHC) in 2012, corresponding to an integrated luminosity of $19.4\,\mathrm{fb}^{-1}$. Previous LHC new-physics searches in final states with b jets and $E_{\mathrm{T}}^{\mathrm{miss}}$ are presented in Refs. [13–25]. The current analysis is an extension of the study presented in Ref. [23], which was based on $5.0\,\mathrm{fb}^{-1}$ of data at $\sqrt{s} = 7\,\mathrm{TeV}$. We retain the same basic analysis procedures, characterized by a strong reliance on control samples in data, to evaluate the SM backgrounds. The principal backgrounds arise from events with a top-antitop ($\mathrm{t\bar{t}}$) quark pair, a single-top quark, a W boson produced in association with jets (W+jets), a Z boson produced in association with jets (Z+jets), and multiple jets produced through the strong interaction (QCD), in which an identified b jet is present. The QCD category excludes events in the other categories. For W+jets events and events with a top quark, significant $E_{\mathrm{T}}^{\mathrm{miss}}$ can arise if a W boson decays into a neutrino and a charged lepton. The neutrino provides a source of genuine $E_{\mathrm{T}}^{\mathrm{miss}}$. For events with a Z boson, significant $E_{\mathrm{T}}^{\mathrm{miss}}$ can arise if the Z boson decays to two neutrinos. For QCD events, significant $E_{\mathrm{T}}^{\mathrm{miss}}$ can arise when a charm or bottom quark undergoes semileptonic decay, but it arises primarily as a consequence of the mismeasurement of jet transverse momentum p_{T}.

As new-physics scenarios, we consider gluino pair production followed by the decay of each gluino $\tilde{\mathrm{g}}$ into a b quark and an off-shell b squark or into a t quark and an off-shell t squark. The off-shell b squark (t squark) decays into a b quark (t quark) and the LSP, where the LSP (taken to be the lightest neutralino $\tilde{\chi}_1^0$) is assumed to escape detection, leading to significant $E_{\mathrm{T}}^{\mathrm{miss}}$. We consider these scenarios in the context of the T1bbbb and T1tttt [26] simplified model spectra (SMS) [27–30], for which event diagrams are shown in Fig. 1. If the b squark (t squark) is much lighter than any other squark, as suggested by natural models of SUSY, with the gluino yet lighter, gluino decays are expected to be dominated by the three-body process of Fig. 1a (Fig. 1b). Our search thus targets NP scenarios with relatively light gluinos and third-generation squarks. The gluino and LSP masses are treated as independent parameters. As ref-

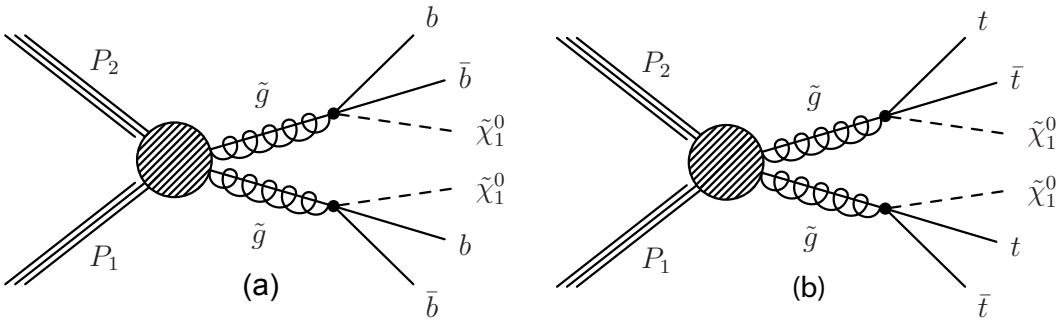

Figure 1: Event diagrams for the (a) T1bbbb and (b) T1tttt simplified model new-physics scenarios.

erence new-physics processes, we consider the T1bbbb and T1tttt scenarios with normalization to the next-to-leading order (NLO) plus next-to-leading-logarithm (NLL) cross section [31–35].

It is rare for a T1bbbb event to contain a high-p_{T} isolated lepton. To define the search region for this study, we therefore veto events with an identified isolated electron or muon. The corresponding collection of events is referred to as the zero-lepton (ZL) or "signal" sample. Besides the ZL sample, control samples are defined in order to evaluate the SM background. To evaluate the top quark and W+jets background (where "top quark" refers to both $\mathrm{t\bar{t}}$ and single-top quark events), we select a top-quark- and W+jets-dominated control sample by requiring the presence of exactly one identified isolated electron or muon. We refer to this sample as the single-lepton (SL) sample. (Top quark and W+jets events are grouped into a single background category because of their similar experimental signatures.) To evaluate the QCD background, we employ the minimum normalized azimuthal angle $\Delta\hat{\phi}_{\mathrm{min}}$ [23] between the $E_{\mathrm{T}}^{\mathrm{miss}}$ vector and one of three highest-p_{T} jets, selecting a QCD-dominated control sample by requiring small values of this variable. We refer to this control sample as the low-$\Delta\hat{\phi}_{\mathrm{min}}$ (LDP) sample. The Z+jets background is evaluated with control samples of $\mathrm{Z} \to \ell^+\ell^-$ ($\ell = \mathrm{e}$ and μ) events. Our analysis is performed in the framework of a global likelihood fit that simultaneously analyzes the signal and background content, accounting for signal contributions to the ZL and control samples in a unified and consistent manner.

In contrast to T1bbbb events, events in the T1tttt scenario are expected to appear in both the ZL and SL samples. Since our global likelihood fitting procedure can account for T1tttt contributions to the control samples, the analysis procedures and background evaluation methods used to examine the T1tttt scenario are essentially the same as those used for the T1bbbb scenario.

This study extends the analysis of Ref. [23] by exploiting the expected differences in shape between the T1bbbb or T1tttt scenarios and each of the SM background components in the distributions of $E_{\mathrm{T}}^{\mathrm{miss}}$, H_{T}, and the number $N_{\mathrm{b-jet}}$ of tagged b jets in an event, where H_{T} is the scalar sum of jet p_{T} values. The data are divided into mutually exclusive bins in these three variables, as indicated schematically in Fig. 2. The $E_{\mathrm{T}}^{\mathrm{miss}}$ and H_{T} distributions are divided into four bins each. The definitions of these bins are given in the table of Fig. 2. For the ZL, SL, and LDP samples, the b-jet multiplicity distribution is divided into three bins, corresponding to $N_{\mathrm{b-jet}} = 1$, 2, or ≥ 3. There are thus 176 mutually exclusive observables in the analysis, 48 each for the ZL, SL, and LDP samples, and 16 each for the $\mathrm{Z} \to \mathrm{e^+e^-}$ and $\mathrm{Z} \to \mu^+\mu^-$ samples, where each observable corresponds to the number of data events in a bin. The contents of the bins are examined simultaneously in the likelihood fit.

This note is organized as follows. In Section 2 we discuss the detector and trigger. Sections 3 and 4 describe the event selection. The likelihood framework and background-determination

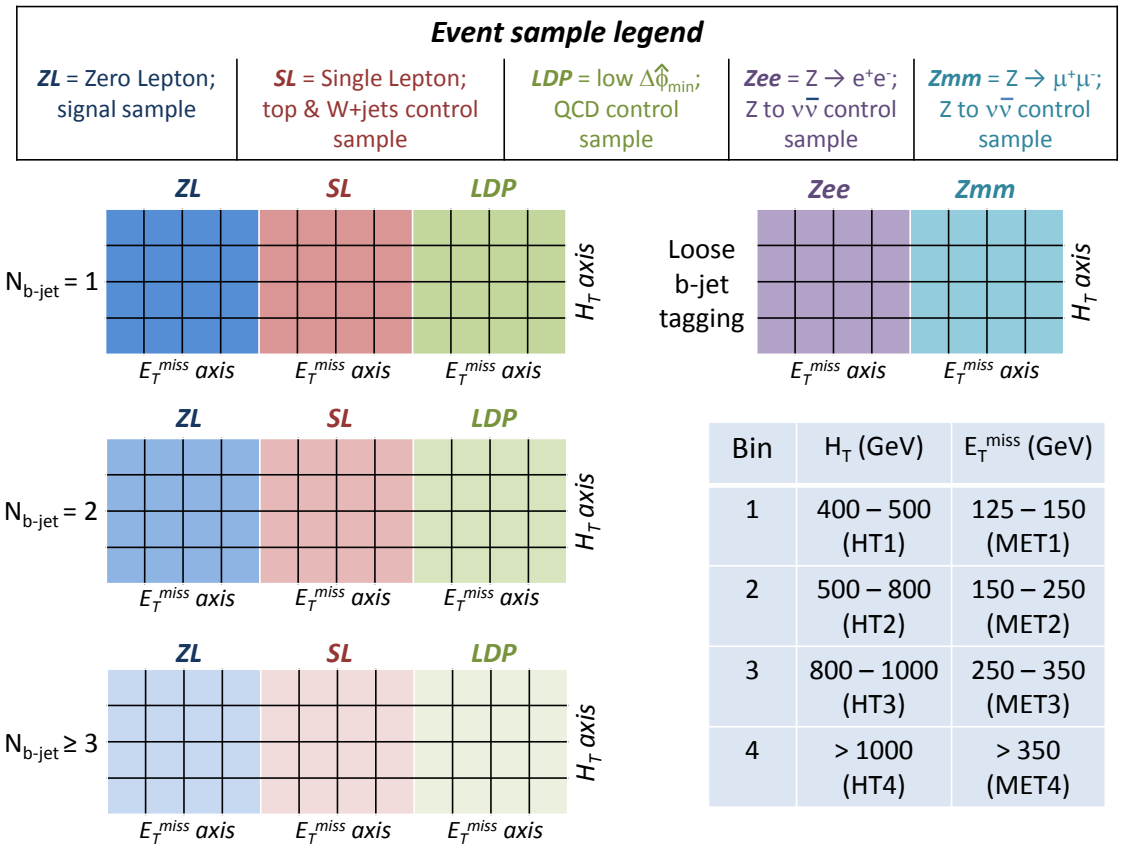

Bin	H_T (GeV)	E_T^{miss} (GeV)
1	400 – 500 (HT1)	125 – 150 (MET1)
2	500 – 800 (HT2)	150 – 250 (MET2)
3	800 – 1000 (HT3)	250 – 350 (MET3)
4	> 1000 (HT4)	> 350 (MET4)

Figure 2: Schematic diagram illustrating the 176 mutually exclusive observables of the analysis. The $E_{\mathrm{T}}^{\mathrm{miss}}$ and H_{T} distributions are divided into four bins each; the table gives the bin definitions. The designations HTi and METi ($i = 1-4$) are used to label the individual H_{T} and $E_{\mathrm{T}}^{\mathrm{miss}}$ bins. The $N_{\mathrm{b-jet}}$ distributions of the signal sample (ZL), top-quark and W+jets control sample (SL), and QCD control sample (LDP), contain three bins each, corresponding to exactly one, exactly two, and three or more identified b jets.

methods are presented in Section 5. Section 6 presents the results and Section 7 a summary.

2 Detector and trigger

A detailed description of the CMS detector is given elsewhere [36]. The CMS coordinate system is defined with the origin at the center of the detector and the z axis along the direction of the counterclockwise beam. The transverse plane is perpendicular to the beam axis, with ϕ the azimuthal angle (measured in radians), θ the polar angle, and $\eta = -\ln[\tan(\theta/2)]$ the pseudorapidity. A superconducting solenoid provides an axial magnetic field of 3.8 T. Within the field volume are a silicon pixel and strip tracker, a crystal electromagnetic calorimeter, and a brass-scintillator hadron calorimeter. The tracking system is completed with muon detectors, based on gas-ionization chambers embedded in the steel flux-return yoke outside the solenoid. The tracking system covers $|\eta| < 2.5$ and the calorimeters $|\eta| < 3.0$. The $3 < |\eta| < 5$ region is instrumented with a forward calorimeter. The near-hermeticity of the detector permits accurate measurements of energy balance in the transverse plane.

Events are selected using multiple trigger conditions, based primarily on thresholds for H_{T} and $E_{\mathrm{T}}^{\mathrm{miss}}$. The trigger efficiency, determined from data, is the probability for an event to satisfy the

trigger conditions. In our analysis, the data are examined in exclusive regions of H_T and E_T^{miss}, as described above. The trigger is found to be nearly 100% efficient except in regions with low values of both H_T and E_T^{miss}. In the bin with lowest H_T and E_T^{miss} (the HT1-MET1 bin of Fig. 2), the evaluated trigger efficiency is 0.91 ± 0.01 (0.86 ± 0.09) for the trigger relevant for the ZL and SL (LDP) samples. Corrections are applied to account for the trigger efficiencies and their corresponding uncertainties.

3 Event Selection

Physics objects are defined with the particle flow (PF) method [37], which is used to reconstruct and identify charged and neutral hadrons, electrons (with associated bremsstrahlung photons), muons, tau leptons, and photons, using an optimized combination of information from CMS subdetectors. The event primary vertex is identified by selecting the reconstructed vertex with the largest scalar sum of charged-track p_T values. Events are required to have a primary vertex with at least four charged tracks and that lies within 24 cm of the origin in the direction along the beam axis and 2 cm in the perpendicular direction. Charged particles used in the analysis must emanate from the primary vertex. In this way, charged particles associated with extraneous pp collisions within the same bunch crossing ("pileup") are disregarded. The PF objects serve as input for jet reconstruction, based on the anti-k_T algorithm [38] with distance parameter 0.5. Jet corrections are applied in both p_T and η to account for residual effects of non-uniform detector response. Additional corrections [39, 40] account for pileup effects from neutral particles. The missing transverse energy E_T^{miss} is defined as the modulus of the vector sum of the transverse momenta of all PF objects. The E_T^{miss} vector is the negative of that same vector sum.

The requirements used to select the zero-lepton (ZL) event sample are as follows:

- at least three jets with $p_T > 50$ GeV and $|\eta| < 2.4$, where the two leading jets satisfy $p_T > 70$ GeV;
- $H_T \geq 400$ GeV, where H_T is calculated using jets with $p_T > 50$ GeV and $|\eta| < 2.4$;
- $E_T^{miss} > 125$ GeV;
- no identified, isolated electron or muon candidate with $p_T > 10$ GeV; electron candidates are restricted to $|\eta| < 2.5$ and muon candidates to $|\eta| < 2.4$;
- no isolated track with $p_T > 15$ GeV and $|\eta| < 2.4$;
- $\Delta\hat{\phi}_{min} > 4.0$, where the $\Delta\hat{\phi}_{min}$ variable is described in Ref. [23];
- at least one tagged b jet, where tagged b jets are required to have $p_T > 50$ GeV and $|\eta| < 2.4$.

The isolated-track requirement eliminates events with an isolated electron or muon in cases where the lepton is not identified, as well as events with a τ-lepton that decays hadronically. Electrons, muons, and tracks are considered isolated if the scalar sum of the p_T values of charged hadrons (for electrons and muons, also photons and neutral hadrons) surrounding the lepton or track within a cone of radius $\sqrt{(\Delta\eta)^2 + (\Delta\phi)^2} = 0.3$ (0.4 for muons), divided by the lepton or track p_T value itself, is less than 0.15, 0.20, and 0.05, respectively.

For the current study, we use a slightly modified definition of the $\Delta\hat{\phi}_{min}$ variable compared to Ref. [23]: we now use "arcsin" rather than "arctan" in the expression for $\sigma_{\Delta\phi,i}$ (see Section IV of Ref. [23]). All other aspects of the $\Delta\hat{\phi}_{min}$ calculation are unchanged. This modification introduces a negligible difference for the small angles relevant here. Nonetheless, arcsin is techni-

cally more correct than arctan.

Identification of b jets is based on the combined-secondary-vertex algorithm at the medium working point [41]. This algorithm combines information about secondary vertices, track impact parameters, and jet kinematics, to separate b jets from light-flavored-quark, charm-quark, and gluon jets. The nominal b-jet tagging efficiency is 75% for jets with a p_{T} value of 80 GeV, as determined from a sample of simulated b-jet-enriched events [41]. The corresponding misidentification rate for light-quark jets is 1.0%.

4 Control samples, search regions, and event simulation

The top-quark- and W+jets-dominated SL control sample is defined by selecting events with exactly one electron or one muon, using the lepton selection criteria and all other nominal selection requirements given in Section 3, with the exception of the requirement that there be no isolated track. To reduce the potential contribution from signal T1tttt events, we apply an additional requirement $m_{\mathrm{T}} < 100\,\mathrm{GeV}$ to the SL sample only, where $m_{\mathrm{T}} = \sqrt{2E_{\mathrm{T}}^{\mathrm{miss}} p_{\mathrm{T}}^{\ell}[1-\cos(\Delta\phi_{\ell,E_{\mathrm{T}}^{\mathrm{miss}}})]}$ is the transverse mass formed from the $E_{\mathrm{T}}^{\mathrm{miss}}$ and p_{T}^{ℓ} (lepton transverse momentum) vectors, with $\Delta\phi_{\ell,E_{\mathrm{T}}^{\mathrm{miss}}}$ the corresponding difference in azimuthal angle.

The region $\Delta\hat{\phi}_{\mathrm{min}} < 4$, with all other nominal selection requirements from Section 3 imposed, defines the QCD-dominated LDP control region.

To evaluate the Z+jets background, we select Z+jets control samples with $\mathrm{Z} \to \mathrm{e}^{+}\mathrm{e}^{-}$ and $\mathrm{Z} \to \mu^{+}\mu^{-}$ decays, as described in Section 5.3.

The data are divided into mutually exclusive bins of $E_{\mathrm{T}}^{\mathrm{miss}}$, H_{T}, and $N_{\mathrm{b-jet}}$, as shown in Fig. 2. This binning is chosen based on simulation studies with SUSY signal and SM background event samples, for which signal sensitivity in the presence of SUSY events, and limits in the absence of such events, are both considered. The best performance is obtained with relatively narrow bins at low H_{T} and $E_{\mathrm{T}}^{\mathrm{miss}}$, which helps to characterize the background shapes, and with multiple bins at high H_{T} and $E_{\mathrm{T}}^{\mathrm{miss}}$, which provides regions with reasonable signal efficiency but very little background. Within this general framework, the sensitivity is found to be relatively independent of particular binning choices.

To illustrate the characteristics of the events, Fig. 3 presents the distribution of $N_{\mathrm{b-jet}}$ for the signal (ZL) and control-region (SL, LDP) samples, and the corresponding distributions of $E_{\mathrm{T}}^{\mathrm{miss}}$ and H_{T} for $N_{\mathrm{b-jet}} \geq 3$. The results are shown in comparison with Monte Carlo (MC) simulations of SM processes. The $\mathrm{t\bar{t}}$, W+jets, and Z+jets MC samples are simulated at the parton level with the MADGRAPH5.1.1.0 [42] event generator. Single-top-quark events are produced with the POWHEG 301 [43] program. The PYTHIA 6.4.22 [44] generator is used for diboson and QCD events. For all SM MC samples, the GEANT4 [45] package is used to model detector response. The top, W+jets, and Z+jets MC distributions are normalized to the next-to-next-to-leading order (NNLO) cross sections. The diboson MC distribution, given by the sum of contributions from WW, WZ, and ZZ events, is normalized to NLO. The QCD distribution is normalized to leading order. We also consider Drell-Yan events, generated with MADGRAPH and normalized to NNLO. The contribution of Drell-Yan events is found to be small (about one fifth or less the contribution from diboson events in all signal regions) and is not included in Fig. 3.

Signal T1bbbb and T1tttt MC samples are generated for a range of gluino m_{gluino} and LSP m_{LSP} mass values using PYTHIA, with $m_{\mathrm{LSP}} < m_{\mathrm{gluino}}$. To reduce computational requirements, signal MC detector response is modeled with the fast simulation program [46]. We account for modest

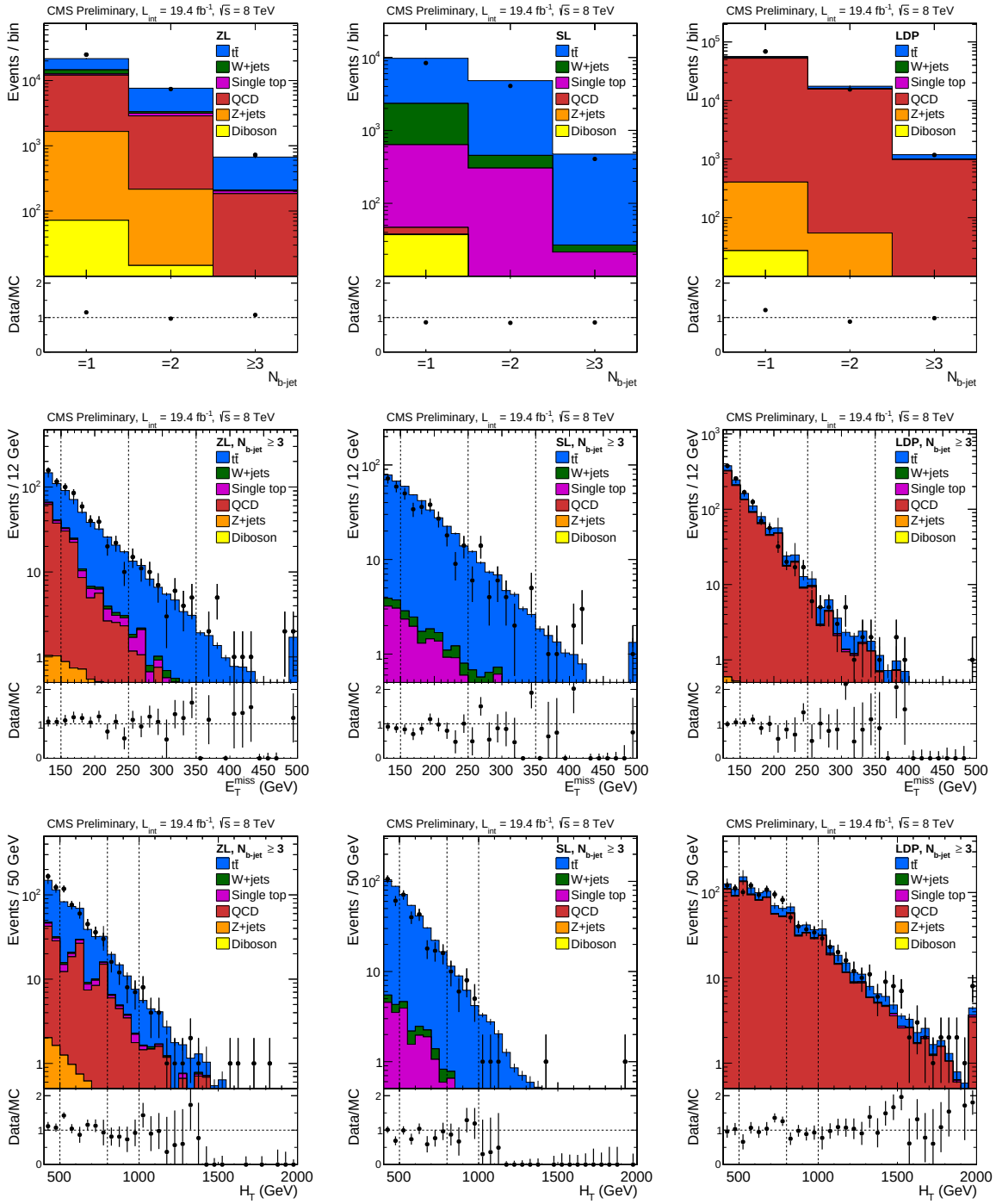

Figure 3: [top row] Data and Monte Carlo distributions of the number $N_{\mathrm{b-jet}}$ of tagged b jets for the [left column] signal (ZL) sample, [center column] top and W+jets (SL) control sample, and [right column] QCD (LDP) control sample. The small lower plots show the ratio of the measured to the simulated events. [center row] Corresponding $E_{\mathrm{T}}^{\mathrm{miss}}$ distributions, and [bottom row] H_{T} distributions, for events with $N_{\mathrm{b-jet}} \geq 3$. The dashed vertical lines indicate the divisions between the four bins of $E_{\mathrm{T}}^{\mathrm{miss}}$ or H_{T}.

differences observed with respect to the GEANT4 simulation.

All MC samples incorporate the CTEQ6 [47] parton distribution functions, with PYTHIA used to describe parton showering and hadronization. The MC distributions are reweighted to account for pileup. In addition, we correct the simulation so that the b-jet tagging and misidentification efficiencies match those determined from control samples in the data. The b-jet tagging efficiency correction factor depends slightly on jet p_{T} and has a typical value of 0.95.

5 Likelihood function and background evaluation methods

In this section, we present the definition of the likelihood function and describe the background evaluation methods.

We use the following notation:

- ZL: the zero-lepton event sample;
- SL: the single-lepton event sample;
- LDP: the low-$\Delta\hat{\phi}_{\mathrm{min}}$ event sample;
- Zee and Zmm: the $\mathrm{Z} \to \mathrm{e}^+\mathrm{e}^-$ and $\mathrm{Z} \to \mu^+\mu^-$ event samples or background components;
- $ttWj$: the top and W+jets background component, where "top" includes both $\mathrm{t\bar{t}}$ and single-top quark events;
- QCD: the QCD background component;
- $Z\nu\nu$: the Z+jets background component;
- $SUSY$: the signal component;
- $\mu^C_{S;i,j,k}$: the estimated number of events in bin i, j, k of event sample S for component C without accounting for trigger efficiency, where i, j, and k denote the bin in $E_{\mathrm{T}}^{\mathrm{miss}}$, H_{T}, and $N_{\mathrm{b-jet}}$, respectively, and C denotes $ttWj$, QCD, or one of the other signal or background terms;
- $n_{S;i,j,k}$: the estimated number of events in bin i, j, k of event sample S from all components after accounting for trigger efficiency;
- $\epsilon^{\mathrm{trig}}_{S;i,j,k}$: the trigger efficiency in bin i, j, k for event sample S;
- $N_{S;i,j,k}$: the observed number of events in bin i, j, k for event sample S.

5.1 Top and W+jets background

The SL sample is used to describe the shape of the top and W+jets background in the three analysis dimensions of $E_{\mathrm{T}}^{\mathrm{miss}}$, H_{T}, and $N_{\mathrm{b-jet}}$. The SL sample thus provides a three-dimensional (3D) histogram-probability-density function (PDF) determined directly from data. The top and W+jets background in each bin of the ZL sample is determined from this measured 3D shape, simulation-derived bin-by-bin corrections $S^{ttWj}_{i,j,k}$, and an overall floating normalization parameter $R^{ttWj}_{ZL/SL}$, as described below.

With respect to SM processes, the SL sample is assumed to be populated by top and W+jets events only. Contributions from QCD and Z+jets events are small (around 1% on average) as seen from Fig. 3, and are accounted for through implementation of a systematic uncertainty. The contribution from T1bbbb events is negligible because isolated leptons are rare in the T1bbbb scenario. In contrast, with four top quarks in the final state, T1tttt events often contain

an isolated high-p_T lepton, resulting in "signal contamination" of the SL sample. Therefore, we presume

$$n_{SL;i,j,k} = \epsilon^{\text{trig}}_{SL;i,j,k} \cdot (\mu^{ttWj}_{SL;i,j,k} + S^{SUSY}_{SL;i,j,k} \cdot \mu^{SUSY}_{SL;i,j,k}) , \quad (1)$$

where $S^{SUSY}_{SL;i,j,k}$ represents a systematic uncertainty, treated as a nuisance parameter. For the T1bbbb scenario, $\mu^{SUSY}_{SL;i,j,k} = 0$.

The three plots in the top row of Fig. 4 show the ratio of the number of top and W+jets events in the ZL sample to the corresponding number in the SL sample, as predicted by simulation, after normalization to the same integrated luminosity. The results are shown for the 48 bins of the ZL and SL samples. Dividing the $N_{\text{b-jet}} = 1$ results shown in the top-left plot by their average, we obtain the normalized ZL-to-SL ratios shown in the bottom-left plot. The bottom-center and bottom-right plots show the corresponding results for $N_{\text{b-jet}} = 2$ and $N_{\text{b-jet}} \geq 3$, respectively. (Note: the average values happen to be very close to one, by coincidence.) Were the 3D shape of top and W+jets events the same in the simulated ZL and SL samples, the points in the top row would all be consistent with a single average value and the points in the bottom row consistent with one. Deviations from one on the order of 20-50% are seen for some points in the bottom row, indicating a shape discrepancy between the two samples. The shape discrepancy is strongest in the H_T dimension. Consistent results are found if the POWHEG or MC@NLO [48] generators are used to describe the $t\bar{t}$ MC sample rather than MADGRAPH.

Our estimate of the top and W+jets contribution to bin i, j, k of the ZL sample is thus

$$\mu^{ttWj}_{ZL;i,j,k} = S^{ttWj}_{i,j,k} \cdot R^{ttWj}_{ZL/SL} \cdot \mu^{ttWj}_{SL;i,j,k} , \quad (2)$$

where $R^{ttWj}_{ZL/SL}$ is the floating scale factor common to all bins mentioned above and the $S^{ttWj}_{i,j,k}$ factors are the MC-based terms presented in the bottom row of Fig. 4, which account for the 3D shape differences between the ZL and SL samples. In the likelihood function, the $S^{ttWj}_{i,j,k}$ terms are treated as floating nuisance parameters, each constrained by a lognormal PDF. The median of the lognormal is the corresponding value shown in the bottom row of Fig. 4, while the geometric standard deviation is $\ln(1 + \sigma_{rel})$, with σ_{rel} the relative uncertainty on the corresponding $S^{ttWj}_{i,j,k}$ term, determined from the quadrature sum of its statistical uncertainty and one half of the difference from one. In addition, we vary the W+jets cross section by 100% [49] and the single-top cross section by 30% [50]. The differences relative to the standard result define uncertainties for lognormal distributions that are applied as additional constraints on the $S^{ttWj}_{i,j,k}$ terms.

5.2 QCD background

The QCD background in each bin of the ZL sample, in the 3D space of E_T^{miss}, H_T, and $N_{\text{b-jet}}$, is determined from the number of events in the corresponding bin of the LDP sample, in conjunction with multiplicative scale factors described below. Before applying these scale factors, the contributions of top and W+jets events are subtracted from the measured LDP results, as are the contributions of Z+jets events. The estimate of the top and W+jets contribution to the LDP sample is derived from the data-based top and W+jets event yield in the ZL sample, found in the likelihood fit (Section 6) for the corresponding bin, multiplied by the MC ratio of LDP to ZL events for that bin, and analogously for the Z+jets contribution to the LDP sample. The uncertainty on this subtraction procedure accounts for the total uncertainty on the respective ZL event yield, and for a 10% uncertainty on the simulated ratio, where the latter uncertainty corresponds to the average statistical uncertainty on the MC ratio values.

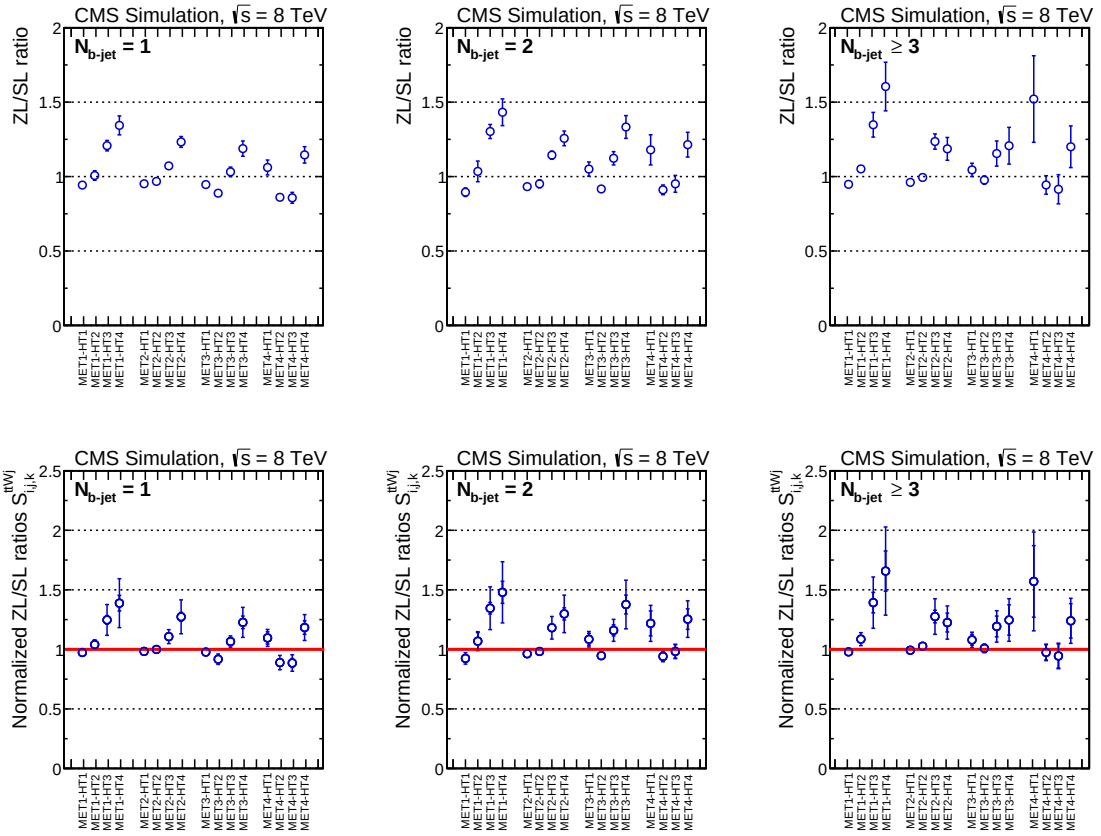

Figure 4: [top row] Ratio of the number of events in the zero-lepton (ZL) sample to the number in the single-lepton (SL) sample for simulated top and W+jets events. The plots from left to right show the results for $N_{\mathrm{b-jet}} = 1$, 2, and ≥ 3, respectively. Within a plot, the leftmost group of four consecutive points corresponds to $E_{\mathrm{T}}^{\mathrm{miss}}$ bin 1 (MET1) of the table in Fig. 2, the next-leftmost group to $E_{\mathrm{T}}^{\mathrm{miss}}$ bin 2 (MET2), etc. The four points within each group correspond to the four H_{T} bins in the table, increasing in H_{T} value from left to right (HT1 to HT4). The uncertainties are statistical. [bottom row] The [left column] $N_{\mathrm{b-jet}} = 1$ results from the top left plot, divided by the average ratio from that same plot, and [center and right columns] the corresponding results for $N_{\mathrm{b-jet}} = 2$ and $N_{\mathrm{b-jet}} \geq 3$. The inner (outer) error bars show the statistical (combined statistical and systematic) uncertainties.

The top row of Fig. 5 shows the ratio between the number of QCD events in the ZL sample to the corresponding number in the LDP sample, as predicted by simulation, after normalization to the same integrated luminosity. The results are shown for the 48 bins of the ZL and LDP samples. This ratio is seen to depend strongly on H_{T}. The dependence on $E_{\mathrm{T}}^{\mathrm{miss}}$ and $N_{\mathrm{b-jet}}$ is more moderate. We parameterize the $E_{\mathrm{T}}^{\mathrm{miss}}$, H_{T}, and $N_{\mathrm{b-jet}}$ dependence assuming that this dependence factorizes, i.e., we take an empirical approach and assume that the H_{T} dependence is independent of $E_{\mathrm{T}}^{\mathrm{miss}}$ and $N_{\mathrm{b-jet}}$, etc. We thus model the QCD background contribution to the ZL sample for a given $E_{\mathrm{T}}^{\mathrm{miss}}$, H_{T}, $N_{\mathrm{b-jet}}$ bin as:

$$\mu^{QCD}_{ZL;i,j,k} = S^{QCD}_{i,j,k} \cdot \left(K^{QCD}_{MET,i} \cdot K^{QCD}_{HT,j} \cdot K^{QCD}_{Nb,k} \right) \cdot \mu^{QCD}_{LDP;i,j,k} \,, \tag{3}$$

where the $S^{QCD}_{i,j,k}$ factors are defined below and the three K^{QCD} terms account for the $E_{\mathrm{T}}^{\mathrm{miss}}$, H_{T}, and $N_{\mathrm{b-jet}}$ dependence. Note that some bins in the top row of Fig. 5 do not contain any entries.

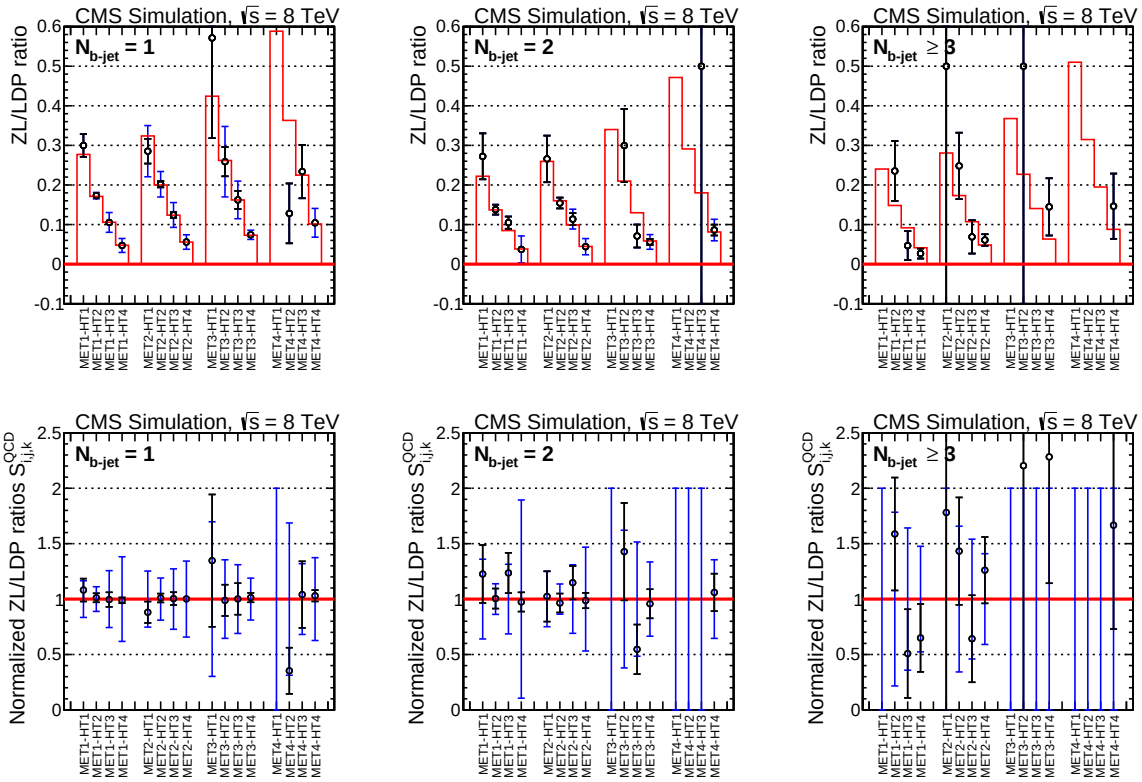

Figure 5: [top row] Ratio of the number of events in the zero-lepton (ZL) sample to the number in the low-$\Delta\hat{\phi}_{\text{min}}$ (LDP) sample for simulated QCD events. The definitions of the bins are the same as in Fig. 4. Various QCD samples, with different choices for the hardness ($\hat{p}_{\text{T}}$ [44]) of the interaction, are combined. The points show the averages over those samples. The inner error bars indicate the statistical uncertainties. The outer error bars indicate the statistical uncertainties added in quadrature with the RMS values over the different $\hat{p}_{\text{T}}$ samples. The histogram shows the results of the fitted parameterization described in the text. [bottom row] The corresponding ratio divided by the parameterization from the top row. The inner (outer) error bars indicate the statistical (combined statistical and systematic) uncertainties.

These bins, with large $E_{\text{T}}^{\text{miss}}$ and small H_{T}, are kinematically unlikely (a large $E_{\text{T}}^{\text{miss}}$ value implies a large H_{T} value) and thus contain few or no MC events.

We fit the parameterization of Eq. (3) to the ratio values shown in the top row of Fig. 5, taking $S_{i,j,k}^{QCD} \equiv 1$ at this stage, to determine simulation-derived values for the K^{QCD} factors (data-based values are determined in the likelihood fit, as described below). The results of this fit are shown by the histograms in the top row of Fig. 5. The simulated QCD ZL-to-LDP ratio divided by the fitted parameterization is shown in the bottom row of Fig. 5: these ratios define the $S_{i,j,k}^{QCD}$ terms. The points in the bottom row are consistent with one, indicating that the empirical parameterization is sufficient. In the likelihood fit, the $S_{i,j,k}^{QCD}$ factors are treated as nuisance parameters constrained by lognormal PDFs. Since the $S_{i,j,k}^{QCD}$ factors are statistically consistent with one, no corrections are applied and thus the medians of the lognormal PDFs are set to one. Geometric standard deviations for the lognormal distributions are determined from the outer error bars in the bottom row of Fig. 5, given by the quadrature sum of the deviation of the $S_{i,j,k}^{QCD}$ factors from one, their statistical uncertainties, and the RMS values found using the different QCD samples described in the Fig. 5 caption. For bins in the top row of Fig. 5 without

any MC entries, we set $S^{QCD}_{i,j,k} = 1$ and assign a 100% uncertainty, as shown in the bottom row of the figure.

In the likelihood analysis, most of the K^{QCD} factors are free parameters in the fit: there is enough shape information that they can be determined directly from the data. However, we find from studies with simulation that the fit is unable to determine $K^{QCD}_{MET,3}$, $K^{QCD}_{MET,4}$, or $K^{QCD}_{Nb,3}$. Instead, lognormal constraints are applied for these three parameters. The median values are set to the corresponding results from simulation and the geometric standard deviations are determined from half the differences $K^{QCD}_{MET,3} - K^{QCD}_{MET,2}$, $K^{QCD}_{MET,4} - K^{QCD}_{MET,2}$, and $K^{QCD}_{Nb,3} - K^{QCD}_{Nb,1}$, respectively. The results of the fit are found to be insensitive to the choice of the geometric standard deviation values.

5.3 $Z \to \nu\bar{\nu}$ background

The Z+jets background is evaluated by reconstructing $Z \to \ell^+\ell^-$ events (ℓ = e or μ). The ℓ^+ and ℓ^- leptons are then removed so that the events emulate Z+jets events with $Z \to \nu\bar{\nu}$. The $Z \to e^+e^-$ and $Z \to \mu^+\mu^-$ samples are divided into 16 bins in the two-dimensional space of E_T^{miss} and H_T, as indicated in Fig. 2.

Fits to the dilepton invariant mass spectra are performed to determine the $Z \to \ell^+\ell^-$ yields. The yields are corrected to account for background, acceptance, and detection efficiency. The acceptance, determined from simulation, accounts for the larger acceptance of $Z \to \nu\bar{\nu}$ events compared to $Z \to \ell^+\ell^-$ events. The efficiency is $\epsilon = \epsilon_{trig} \cdot \epsilon^2_{\ell\,reco} \cdot \epsilon^2_{\ell\,sel}$, where the trigger ϵ_{trig}, lepton reconstruction $\epsilon_{\ell\,reco}$, and lepton selection $\epsilon_{\ell\,sel}$ factors are determined from data.

The $Z \to \ell^+\ell^-$ yields are small in some of the signal regions. To increase these yields, we select events with the requirements of Section 3 except with a significantly looser b-jet tagging definition. The yield in each bin from this sample is multiplied by an extrapolation factor given by the ratio of the sum of the $Z \to \ell^+\ell^-$ yields over all H_T and E_T^{miss} bins for events that satisfy the nominal b-jet tagging requirements to those that satisfy the loose requirements.

To establish whether the extrapolation factors themselves exhibit a dependence on H_T or E_T^{miss}, we define a control sample with the same loosened b-jet tagging definition, but without requiring the presence of a Z boson. We further require $\Delta\hat{\phi}_{min} < 4.0$, which yields a control sample with a b-jet content similar to that of $Z \to \ell^+\ell^-$ and $Z \to \nu\bar{\nu}$ events. All other selection criteria are the same as for the ZL sample. We verify that the output of the b-jet tagging algorithm is independent of the presence of a Z. From this control sample we find that the extrapolation factor is independent of H_T and E_T^{miss} for $N_{b-jet} = 2$ and $N_{b-jet} \geq 3$. For $N_{b-jet} = 1$ the data show a variation with E_T^{miss} up to 25%; we apply this variation as a correction to the $N_{b-jet} = 1$ extrapolation factors.

The Z+jets background in the $i = E_T^{miss}$, $j = H_T$ bin of the ZL sample with $N_{b-jet} = 1$ is related to the corresponding bin in the $Z \to e^+e^-$ and $Z \to \mu^+\mu^-$ control samples through

$$\mu^{Zee}_{Zee;i,j} = \left(\mu^{Z\nu\nu}_{ZL;i,j,1} \cdot S_{ee} \cdot A_{ee;i} \cdot \epsilon_{ee}\right) / \left(\mathcal{F}_{Z\nu\nu;1} \cdot R_B\right); \quad (4)$$

$$\mu^{Z\mu\mu}_{Z\mu\mu;i,j} = \left(\mu^{Z\nu\nu}_{ZL;i,j,1} \cdot S_{\mu\mu} \cdot A_{\mu\mu;i} \cdot \epsilon_{\mu\mu}\right) / \left(\mathcal{F}_{Z\nu\nu;1} \cdot R_B\right), \quad (5)$$

where $A_{\ell\ell;i}$ and $\epsilon_{\ell\ell}$ are the acceptances and efficiencies for the $Z \to \ell^+\ell^-$ samples, respectively, $S_{\ell\ell}$ is a scale factor to account for systematic uncertainties, $R_B = 5.95 \pm 0.02$ is the ratio of the $Z \to \nu\bar{\nu}$ to the $Z \to \ell^+\ell^-$ branching fraction [51], and $\mathcal{F}_{Z\nu\nu;1}$ is the extrapolation factor that relates the $N_{b-jet} = 1$ selection efficiency to the efficiency of the loose b-jet tagging requirement.

The estimates of the Z+jets background for $N_{\mathrm{b-jet}} = 2$ and $N_{\mathrm{b-jet}} \geq 3$ are given by the $N_{\mathrm{b-jet}} = 1$ result through the ratio of b-jet tagging extrapolation factors:

$$\mu^{Z\nu\nu}_{ZL;i,j,k} \;=\; \mu^{Z\nu\nu}_{ZL;i,j,1} \cdot (\mathcal{F}_{Z\nu\nu;k}/\mathcal{F}_{Z\nu\nu;1}) \;, \tag{6}$$

where k is the $N_{\mathrm{b-jet}}$ bin index.

5.4 Other backgrounds

Backgrounds from diboson and Drell-Yan processes are accounted for using simulation, with an uncertainty of 100%. Their total contribution is 1% or less in all search regions.

5.5 Systematic uncertainties

Systematic uncertainties on the signal efficiency arise from various sources. A systematic uncertainty associated with the jet energy scale is evaluated by varying this scale by its p_{T}- and η-dependent uncertainties. The size of this uncertainty depends on the event kinematics, i.e., the $E_{\mathrm{T}}^{\mathrm{miss}}$ bin, the H_{T} bin, and the assumed values of the gluino and LSP masses: typical values are in the range of 5-10%. A systematic uncertainty of 1% is associated with unclustered energy. This uncertainty is evaluated by varying the transverse energy in an event not clustered into a physics object by 10%. A systematic uncertainty of 3% is associated with anomalous $E_{\mathrm{T}}^{\mathrm{miss}}$ values, caused by events that are misreconstructed or that contain beam-related background. This uncertainty is defined by 100% of the change in efficiency when software filters are applied to reject these events. The uncertainty on the luminosity determination is 4.4% [52]. The systematic uncertainties associated with corrections to the jet energy resolution, the pileup-reweighting procedure mentioned in Section 3, the trigger efficiency, and the b-jet tagging efficiency scale factor, are evaluated by varying the respective quantities by their uncertainties, while systematic uncertainties associated with the parton distribution functions are evaluated following the recommendations of Ref. [53]. The jet energy resolution and pileup-reweighting uncertainties are 2% and 3%, respectively. The uncertainty on the trigger efficiency is generally below 2%. Uncertainties associated with the parton distribution functions are typically below 10%, while those associated with the b-jet tagging efficiency are generally below around 15%. The uncertainties associated with the jet energy scale, b-jet tagging efficiency, and parton distribution functions vary significantly with the event kinematics and are evaluated point-by-point in the scans over gluino and LSP masses discussed in Section 6.

Systematic uncertainties on the background predictions are described in the previous sections. Note that, for our analysis, systematic uncertainties are generally dominated by statistical uncertainties, generated by the limited number of events in the data control samples.

5.6 The global likelihood function

The likelihood function is the product of Poisson PDFs, one for each observable, and the constraint PDFs for the nuisance parameters. For each observable, the Poisson PDF gives the probability to observe N events, given a mean n, where n depends on the floating parameters of the likelihood fit. The region with $E_{\mathrm{T}}^{\mathrm{miss}} > 350\,\mathrm{GeV}$ and $400 < H_{\mathrm{T}} < 500\,\mathrm{GeV}$, representing the bin with highest $E_{\mathrm{T}}^{\mathrm{miss}}$ and lowest H_{T} in our analysis (the HT1-MET4 bin of Fig. 2), is at an extreme limit of phase space and is very sparsely populated, making it difficult to validate our data-based background-evaluation procedures. Furthermore, very few signal events are expected in this region. We therefore exclude the HT1-MET4 bin from the likelihood analysis, corresponding to 11 of the 176 observables. Thus, the effective number of observables in the analysis is 165.

For both signal and background terms, external input parameters are allowed to float and are constrained by a PDF in the likelihood. Parameters with values between zero and one, such as efficiencies, are constrained by beta-distribution PDFs. All others are constrained by lognormal PDFs. Correlations between the different kinematic regions, including the $N_{\mathrm{b-jet}}$ bins, are taken into account. The test statistic is $q_\mu = -2\ln\left(\mathcal{L}_\mu/\mathcal{L}_{\mathrm{max}}\right)$, where $\mathcal{L}_{\mathrm{max}}$ is the maximum likelihood determined by floating all parameters including the signal strength μ, and $\mathcal{L}_\mu$ is the maximum likelihood for a fixed signal strength.

6 Results

Tables 1 and 2 and Fig. 6 present the results of the fit for the 14 bins of the analysis that are most sensitive to the T1bbbb and T1tttt scenarios: the three bins with $H_{\mathrm{T}} > 500\,\mathrm{GeV}$, $E_{\mathrm{T}}^{\mathrm{miss}} > 350\,\mathrm{GeV}$, and $N_{\mathrm{b-jet}} = 2$, for which the results are shown in Table 1, and the 11 bins with $E_{\mathrm{T}}^{\mathrm{miss}} > 150\,\mathrm{GeV}$ and $N_{\mathrm{b-jet}} \geq 3$, for which the results are shown in Table 2. The top row of Table 1 and top section of Table 2 show the number of events observed in the data. The second row or section shows the SM background predictions obtained from the fit, which are seen to be in agreement with the data to within the uncertainties. The bottom row or section presents the background predictions from the simulation.

Table 1: Observed number of events, SM background estimates from the fit, and expectations from Monte Carlo simulation, for events with $E_{\mathrm{T}}^{\mathrm{miss}} > 350\,\mathrm{GeV}$ and $N_{\mathrm{b-jet}} = 2$. The labels HT2, HT3, and HT4 refer to the bins of H_{T} indicated in Fig. 2, while HT2-4 is the sum over the three bins.

$N_{\mathrm{b-jet}} = 2$, MET4	HT2	HT3	HT4	HT2-4
Observed number of events	66	19	19	104
SM background predictions from fit	$70.5\,^{+6.3}_{-5.9}$	$20.7\,^{+3.2}_{-2.8}$	$19.0\,^{+3.2}_{-2.8}$	110 ± 8
SM background predictions from simulation	81.6 ± 1.9	28.7 ± 1.3	23.3 ± 0.8	134 ± 2

The Appendix presents results from a "sideband fit" in which the 14 bins of Tables 1 and 2 are excluded from the likelihood analysis.

Upper limits on the cross sections to produce events in the T1bbbb and T1tttt scenarios are determined at 95% confidence level. The limits are based on the $\mathrm{CL_s}$ [55, 56] procedure and are presented as a function of the gluino and LSP masses. Using the NLO+NLL cross section as a reference, we also evaluate the corresponding 95% confidence level exclusion curves. The results are shown in Fig. 7. We do not include results within 175 GeV of the $m_{\mathrm{gluino}} = m_{\mathrm{LSP}}$ diagonal because of neglected uncertainties from initial-state radiation, which are large in this region. In the context of the T1bbbb scenario, conservatively using the minus-one-standard-deviation result [54] for the reference cross section, we exclude gluinos with masses below 1150 GeV for LSP masses below 500 GeV. For smaller LSP (gluino) masses, gluinos (LSPs) below 1200 GeV (620 GeV) are excluded. For the T1tttt scenario, gluinos with masses below 1000 GeV are excluded for LSP masses below 250 GeV, with gluino (LSP) mass values below 1020 GeV (300 GeV) excluded for smaller LSP (gluino) masses. While these limits do not exclude the entire range of gluino masses $m_{\tilde{\mathrm{g}}} \lesssim 1.5\,\mathrm{TeV}$ suggested by natural models of SUSY [11], they are nonetheless amongst the most stringent bounds that have yet been obtained and greatly improve our results from Ref. [23].

Table 2: Observed number of events, SM background estimates from the fit, and expectations from Monte Carlo simulation, for events with $E_{\mathrm{T}}^{\mathrm{miss}} > 150\,\mathrm{GeV}$ and $N_{\mathrm{b-jet}} \geq 3$. The labels HT1, HT2, MET2, etc., refer to the bins of H_{T} and $E_{\mathrm{T}}^{\mathrm{miss}}$ indicated in Fig. 2. HT1-4 (MET2-4) refers to the sum over the four H_{T} (three $E_{\mathrm{T}}^{\mathrm{miss}}$) bins. The HT1-MET4 bin is excluded from the analysis, as explained in Section 5.6.

Observed number of events					
$N_{\mathrm{b-jet}} \geq 3$	HT1	HT2	HT3	HT4	HT1-4
MET2	161	182	18	14	375
MET3	15	36	6	4	61
MET4	—	8	2	4	14
MET2-4	176	226	26	22	450
SM background predictions from fit					
$N_{\mathrm{b-jet}} \geq 3$	HT1	HT2	HT3	HT4	HT1-4
MET2	$157\,^{+13}_{-12}$	$179\,^{+13}_{-12}$	$23.2\,^{+3.8}_{-3.4}$	$12.3\,^{+2.7}_{-2.3}$	$372\,^{+19}_{-18}$
MET3	$15.5\,^{+3.0}_{-2.6}$	$32.1\,^{+4.3}_{-3.8}$	$5.9\,^{+1.9}_{-1.5}$	$2.9\,^{+1.3}_{-1.0}$	$56.5\,^{+5.7}_{-5.4}$
MET4	—	$8.4\,^{+2.1}_{-1.8}$	$2.0\,^{+1.0}_{-0.7}$	$2.1\,^{+1.1}_{-0.9}$	$12.4\,^{+2.5}_{-2.2}$
MET2-4	$173\,^{+13}_{-12}$	$220\,^{+14}_{-13}$	$31.0\,^{+4.3}_{-3.8}$	$17.3\,^{+3.1}_{-2.8}$	$441\,^{+20}_{-19}$
SM background predictions from simulation					
$N_{\mathrm{b-jet}} \geq 3$	HT1	HT2	HT3	HT4	HT1-4
MET2	127 ± 8	180 ± 12	27 ± 2	13 ± 1	347 ± 14
MET3	14.7 ± 0.7	30.9 ± 0.7	7.5 ± 0.4	3.9 ± 0.2	56.9 ± 2.6
MET4	—	6.1 ± 0.2	2.6 ± 0.2	2.6 ± 0.2	11.3 ± 0.3
MET2-4	141 ± 8	217 ± 12	37 ± 2	20 ± 1	415 ± 15

7 Summary

A search is presented for an anomalous rate of events with three or more jets, at least one bottom-quark jet, no identified isolated electron or muon, and large missing transverse energy. The search is based on a sample of proton-proton collision data collected at $\sqrt{s} = 8\,\mathrm{TeV}$ with the CMS detector at the LHC in 2012, corresponding to an integrated luminosity of $19.4\,\mathrm{fb}^{-1}$. The principal standard model backgrounds, from events with top quarks, W bosons and jets, Z bosons and jets, and QCD-multijet production, are evaluated using control samples in the data. The analysis is performed in the framework of a global likelihood fit in which the number of events in 165 exclusive bins in a three-dimensional array of missing transverse energy, the number of tagged b jets, and the scalar sum of jet p_{T} values, are simultaneously examined. The background predictions are found to agree with the observed numbers of events to within the uncertainties. We interpret the results in the context of simplified-model-spectra new-physics scenarios in which gluino pair production is followed by the decay of each gluino to two bottom quarks, or two top quarks, and an undetected particle. We set 95% confidence level upper limits on the cross sections for these scenarios. For the T1bbbb scenario, using the NLO+NLL cross

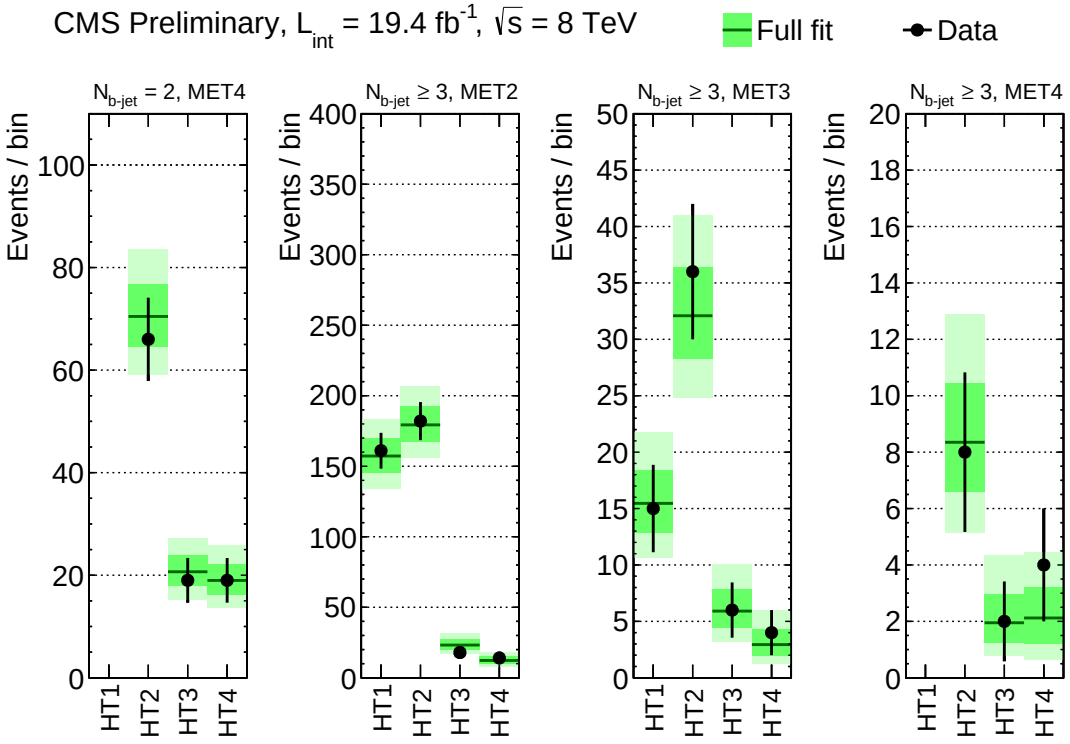

Figure 6: Observed number of events (points with error bars) for the 14 bins with highest signal sensitivity in the analysis. The dark- and light-shaded bands indicate the ± 1 and ± 2 standard deviation intervals, respectively, for the SM background estimates from the fit.

section as a reference, we exclude gluinos with masses below around 1150 GeV for LSP masses below 500 GeV. For the T1tttt scenario, gluinos with masses below 1000 GeV are excluded for LSP masses below 250 GeV.

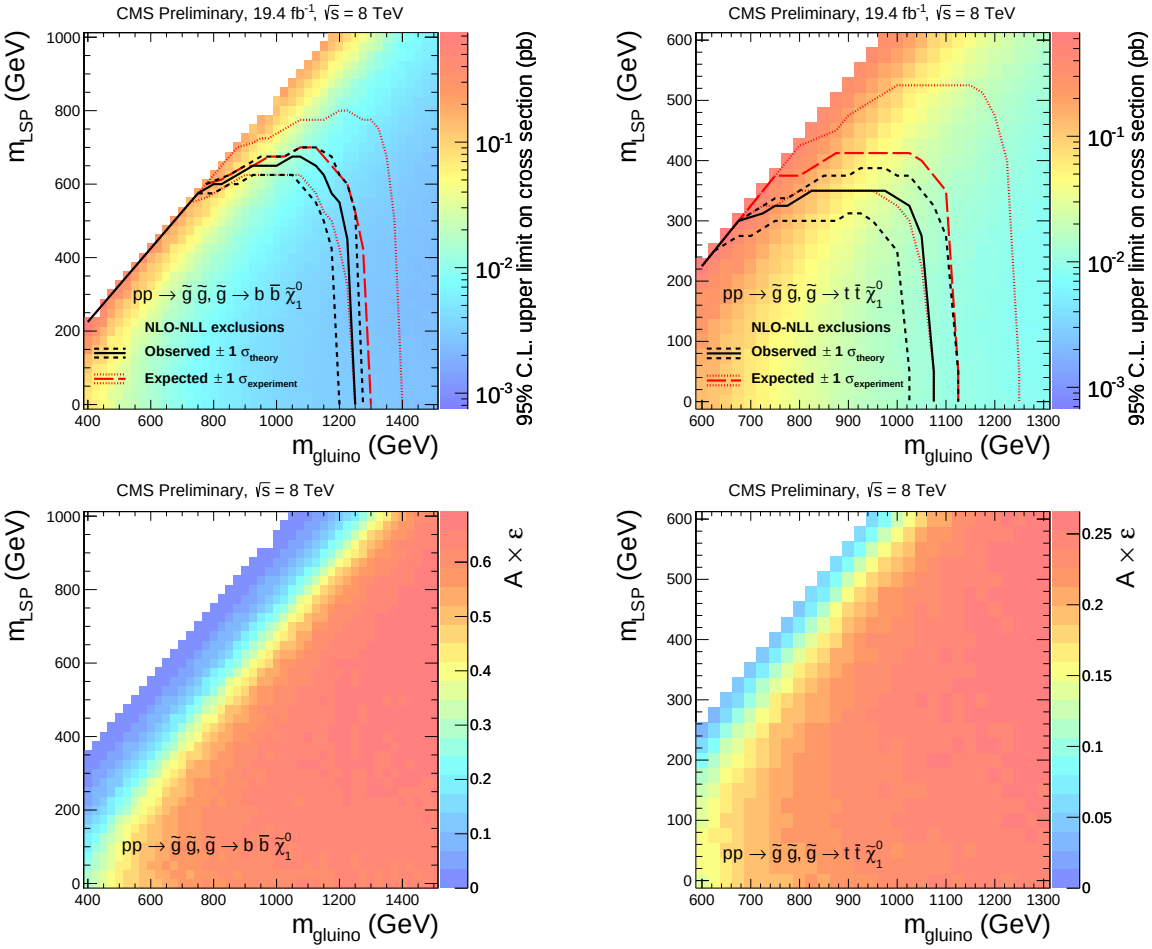

Figure 7: [top row] 95% confidence level (C.L.) upper limits on the [left column] T1bbbb and [right column] T1tttt new physics scenario cross sections (pb) derived using the CL_s method. The solid (black) contours show the observed exclusions assuming the NLO+NLL cross sections [31–35], along with the ± 1 standard deviation theory uncertainties [54]. The long-dashed (red) contours present the corresponding expected results, along with the ± 1 standard deviation experimental uncertainties. Results within 175 GeV of the $m_{\text{gluino}} = m_{\text{LSP}}$ diagonal are excluded as explained in the text. [bottom row] The corresponding selection efficiencies.

References

[1] P. Ramond, "Dual theory for free fermions", *Phys. Rev. D* **3** (1971) 2415, doi:10.1103/PhysRevD.3.2415.

[2] Y. Golfand and E. Likhtman, "Extension of the algebra of Poincaré group generators and violation of p invariance", *JETP Lett.* **13** (1971) 323.

[3] A. Neveu and J. Schwarz, "Factorizable dual model of pions", *Nucl. Phys. B* **31** (1971) 86, doi:10.1016/0550-3213(71)90448-2.

[4] D. Volkov and V. Akulov, "Possible universal neutrino interaction", *JETP Lett.* **16** (1972) 438.

[5] J. Wess and B. Zumino, "A Lagrangian model invariant under supergauge transformations", *Phys. Lett. B* **49** (1974) 52, doi:10.1016/0370-2693(74)90578-4.

[6] J. Wess and B. Zumino, "Supergauge transformations in four dimensions", *Nucl. Phys. B* **70** (1974) 39, doi:10.1016/0550-3213(74)90355-1.

[7] P. Fayet, "Supergauge invariant extension of the Higgs mechanism and a model for the electron and its neutrino", *Nucl. Phys. B* **90** (1975) 104, doi:10.1016/0550-3213(75)90636-7.

[8] H. P. Nilles, "Supersymmetry, supergravity and particle physics", *Phys. Rep.* **110** (1984) 1, doi:10.1016/0370-1573(84)90008-5.

[9] S. Dimopoulos and G. Giudice, "Naturalness constraints in supersymmetric theories with nonuniversal soft terms", *Phys. Lett. B* **357** (1995) 573, doi:10.1016/0370-2693(95)00961-J.

[10] R. Barbieri and D. Pappadopulo, "S-particles at their naturalness limits", *J. High Energy Phys.* **10** (2009) 061, doi:10.1088/1126-6708/2009/10/061.

[11] M. Papucci, J. T. Ruderman, and A. Weiler, "Natural SUSY endures", *J. High Energy Phys.* **09** (2012) 035, doi:10.1007/JHEP09(2012)035.

[12] G. R. Farrar and P. Fayet, "Phenomenology of the production, decay, and detection of new hadronic states associated with supersymmetry", *Phys. Lett. B* **76** (1978) 575, doi:10.1016/0370-2693(78)90858-4.

[13] ATLAS Collaboration, "Search for supersymmetry in pp collisions at $\sqrt{s} = 7$ TeV in final states with missing transverse momentum and b jets", *Phys. Lett.* **B701** (2011) 398, doi:10.1016/j.physletb.2011.06.015.

[14] ATLAS Collaboration, "Search for scalar bottom pair production with the ATLAS detector in pp Collisions at $\sqrt{s} = 7$ TeV", *Phys. Rev. Lett.* **108** (2012) 181802, doi:10.1103/PhysRevLett.108.181802.

[15] ATLAS Collaboration, "Search for supersymmetry in pp collisions at $\sqrt{s} = 7$ TeV in final states with missing transverse momentum and b jets with the ATLAS detector", *Phys. Rev. D* **85** (2012) 112006, doi:10.1103/PhysRevD.85.112006.

[16] ATLAS Collaboration, "Search for top and bottom squarks from gluino pair production in final states with missing transverse energy and at least three b jets with the ATLAS detector", *Eur. Phys. J. C* **72** (2012) 2174, doi:10.1140/epjc/s10052-012-2174-z.

[17] ATLAS Collaboration, "Search for a supersymmetric partner to the top quark in final states with jets and missing transverse momentum at $\sqrt{s} = 7$ TeV with the ATLAS detector", *Phys. Rev. Lett.* **109** (2012) 211802, doi:10.1103/PhysRevLett.109.211802.

[18] ATLAS Collaboration, "Search for direct top squark pair production in final states with one isolated lepton, jets, and missing transverse momentum in $\sqrt{s} = 7$ TeV pp collisions using 4.7 fb^{-1} of ATLAS data", *Phys. Rev. Lett.* **109** (2012) 211803, doi:10.1103/PhysRevLett.109.211803.

[19] ATLAS Collaboration, "Search for light top squark pair production in final states with leptons and b jets with the ATLAS detector in $\sqrt{s} = 7$ TeV proton-proton collisions", arXiv:1209.2102. Submitted to *Phys. Lett. B*.

[20] CMS Collaboration, "Search for supersymmetry in events with b jets and missing transverse momentum at the LHC", *J. High Energy Phys.* **07** (2011) 113, doi:10.1007/JHEP07(2011)113.

[21] CMS Collaboration, "Search for new physics in events with same-sign dileptons and b-tagged jets in pp collisions at $\sqrt{s} = 7$ TeV", *J. High Energy Phys.* **08** (2012) 110, doi:10.1007/JHEP08(2012)110.

[22] CMS Collaboration, "Search for supersymmetry in hadronic final states using MT_2 in pp collisions at $\sqrt{s} = 7$ TeV", *J. High Energy Phys.* **10** (2012) 018, doi:10.1007/JHEP10(2012)018.

[23] CMS Collaboration, "Search for supersymmetry in events with b-quark jets and missing transverse energy in pp collisions at 7 TeV", *Phys. Rev. D* **86** (2012) 072010, doi:10.1103/PhysRevD.86.072010.

[24] CMS Collaboration, "Search for supersymmetry in final states with missing transverse energy and 0, 1, 2, or at least 3 b-quark jets in 7 TeV pp collisions using the variable α_T", *J. High Energy Phys.* **01** (2013) 077, doi:10.1007/JHEP01(2013)077.

[25] CMS Collaboration, "Search for supersymmetry in final states with a single lepton, b-quark jets, and missing transverse energy in proton-proton collisions at $\sqrt{s} = 7$ TeV", arXiv:1211.3143. Submitted to *Phys. Rev. D*.

[26] CMS Collaboration, "Interpretation of searches for supersymmetry with simplified models", arXiv:1301.2175. Submitted to *Phys. Rev. D.*

[27] N. Arkani-Hamed et al., "MARMOSET: The path from LHC data to the new standard model via on-shell effective theories", (2007). arXiv:hep-ph/0703088.

[28] J. Alwall, P. Schuster, and N. Toro, "Simplified models for a first characterization of new physics at the LHC", *Phys. Rev. D* **79** (2009) 075020, doi:10.1103/PhysRevD.79.075020.

[29] J. Alwall et al., "Model-independent jets plus missing energy searches", *Phys. Rev. D* **79** (2009) 015005, doi:10.1103/PhysRevD.79.015005.

[30] D. Alves et al., "Simplified models for LHC new physics searches", *J. Phys. G* **39** (2012) 105005, doi:10.1088/0954-3899/39/10/105005.

[31] W. Beenakker et al., "Squark and gluino production at hadron colliders", *Nucl. Phys. B* **492** (1997) 51, doi:10.1016/S0550-3213(97)00084-9.

[32] A. Kulesza and L. Motyka, "Threshold resummation for squark-antisquark and gluino-pair production at the LHC", *Phys. Rev. Lett.* **102** (2009) 111802, doi:10.1103/PhysRevLett.102.111802.

[33] A. Kulesza and L. Motyka, "Soft gluon resummation for the production of gluino-gluino and squark-antisquark pairs at the LHC", *Phys. Rev. D* **80** (2009) 095004, doi:10.1103/PhysRevD.80.095004.

[34] W. Beenakker et al., "Soft-gluon resummation for squark and gluino hadroproduction", *J. High Energy Phys.* **12** (2009) 041, doi:10.1088/1126-6708/2009/12/041.

[35] W. Beenakker et al., "Squark and gluino hadroproduction", *Int. J. Mod. Phys. A* **26** (2011) 2637, doi:10.1142/S0217751X11053560.

[36] CMS Collaboration, "The CMS experiment at the CERN LHC", *Journal of Instrum.* **03** (2008) S08004, doi:10.1088/1748-0221/3/08/S08004.

[37] CMS Collaboration, "Particle flow event reconstruction in CMS and performance for jets, taus and $E_{\mathrm{T}}^{\mathrm{miss}}$", CMS Physics Analysis Summary CMS-PAS-PFT-09-001, (2009).

[38] M. Cacciari, G. P. Salam, and G. Soyez, "The anti-k_t jet clustering algorithm", *J. High Energy Phys.* **04** (2008) 063, doi:10.1088/1126-6708/2008/04/063.

[39] CMS Collaboration, "Determination of jet energy calibration and transverse momentum resolution in CMS", *JINST* **6** (2011) P11002, doi:10.1088/1748-0221/6/11/P11002.

[40] M. Cacciari, G. P. Salam, and G. Soyez, "FastJet user manual", *Eur. Phys. J. C* **72** (2012) 1896, doi:10.1140/epjc/s10052-012-1896-2.

[41] CMS Collaboration, "Identification of b-quark jets with the CMS experiment", arXiv:1211.4462. Submitted to *Journal of Instrum.*

[42] J. Alwall et al., "MadGraph5: going beyond", *J. High Energy Phys.* **06** (2011) 128, doi:10.1007/JHEP06(2011)128.

[43] S. Frixione, P. Nason, and C. Oleari, "Matching NLO QCD computations with parton shower simulations: the POWHEG method", *J. High Energy Phys.* **11** (2007) 070, doi:10.1088/1126-6708/2007/11/070.

[44] T. Sjöstrand, S. Mrenna, and P. Skands, "PYTHIA 6.4 physics and manual", *J. High Energy Phys.* **05** (2006) 026, doi:10.1088/1126-6708/2006/05/026.

[45] S. Agostinelli et al., "GEANT4—a simulation toolkit", *Nucl. Instr. and Meth. A* **506** (2003) 250, doi:10.1016/S0168-9002(03)01368-8.

[46] CMS Collaboration, "Comparison of the fast simulation of CMS with the first LHC data", CMS Detector Performance Summary CMS-DP-2010-039, (2010).

[47] J. Pumplin et al., "New generation of parton distributions with uncertainties from global QCD analysis", *J. High Energy Phys.* **07** (2002) 12, doi:10.1088/1126-6708/2002/07/012.

[48] S. Frixione and B. R. Webber, "Matching NLO QCD computations and parton shower simulations", *J. High Energy Phys.* **06** (2002) 029, doi:10.1088/1126-6708/2002/06/029.

[49] ATLAS Collaboration, "Measurement of the cross section for the production of a W boson in association with b jets in pp collisions at $\sqrt{s} = 7$ TeV with the ATLAS detector", *Phys. Lett. B* **707** (2012) 418, doi:10.1016/j.physletb.2011.12.046.

[50] CMS Collaboration, "Evidence for associated production of a single top quark and W boson in pp collisions at 7 TeV", *Phys. Rev. Lett.* **110** (2013) 022003, doi:10.1103/PhysRevLett.110.022003.

[51] Particle Data Group Collaboration, "Review of particle physics", *Phys. Rev. D.* **86** (2012) 010001, doi:10.1103/PhysRevD.86.010001.

[52] CMS Collaboration, "CMS luminosity based on pixel cluster counting – summer 2012 update", CMS Physics Analysis Summary CMS-PAS-LUM-12-001, (2012).

[53] M. Botje et al., "The PDF4LHC working group interim recommendations", (2011). arXiv:1101.0538.

[54] M. Krämer et al., "Supersymmetry production cross sections in pp collisions at $\sqrt{s} = 7$ TeV", (2012). arXiv:1206.2892.

[55] T. Junk, "Confidence level computation for combining searches with small statistics", *Nucl. Instr. and Meth. A* **434** (1999) 435, doi:10.1016/S0168-9002(99)00498-2.

[56] A. L. Read, "Presentation of search results: the CL_s technique", *J. Phys. G* **28** (2002) 2693, doi:10.1088/0954-3899/28/10/313.

A Results from a sideband fit

The likelihood fit presented in Section 6 includes the 14 bins with highest signal sensitivity to the T1bbbb and T1tttt new physics scenarios. These bins are indicated in Tables 1 and 2. It is interesting to perform the likelihood fit with the Poisson PDF terms for these 14 bins removed, in order to ascertain the data-based SM background prediction when the data in these bins do not affect the result. We call such a fit the "sideband" fit. The sideband fit is therefore based on 151 observables.

The sideband fit predictions for the SM background in these 14 "most-sensitive" bins are presented in Tables 3 and 4 and in Fig. 8. In comparison with the corresponding results from Section 6, the deviations with respect to the data are somewhat larger. The largest deviation between observation and SM expectation occurs for the bin with $N_{\mathrm{b-jet}} \geq 3$, $H_{\mathrm{T}} > 1000\,\mathrm{GeV}$, and $E_{\mathrm{T}}^{\mathrm{miss}} > 350\,\mathrm{GeV}$ (the HT4-MET4 bin of Table 4), where 4 events are observed whereas only $0.4^{+0.6}_{-0.2}$ events are expected (note that these uncertainties are not Gaussian). From studies with ensembles of simulated experiments, we estimate the probability for a fluctuation in the background in this bin to match or exceed 4 events to be 9% and do not consider it further.

Table 3: SM background estimates from the sideband fit for events with $E_{\mathrm{T}}^{\mathrm{miss}} > 350\,\mathrm{GeV}$ and $N_{\mathrm{b-jet}} = 2$. The labels HT2, HT3, and HT4 refer to the bins of H_{T} indicated in Fig. 2, while HT2-4 is the sum over the three bins.

$N_{\mathrm{b-jet}} = 2$, MET4	HT2	HT3	HT4	HT2-4
Sideband-fit SM background predictions	$76.4\,^{+10.2}_{-9.1}$	$22.3\,^{+4.5}_{-3.9}$	$19.0\,^{+4.5}_{-3.7}$	$118\,^{+13}_{-12}$

Table 4: SM background estimates from the sideband fit for events with $E_{\mathrm{T}}^{\mathrm{miss}} > 150\,\mathrm{GeV}$ and $N_{\mathrm{b-jet}} \geq 3$. The labels HT1, HT2, MET2, etc., refer to the bins of H_{T} and $E_{\mathrm{T}}^{\mathrm{miss}}$ indicated in Fig. 2. HT1-4 (MET2-4) refers to the sum over the four H_{T} (three $E_{\mathrm{T}}^{\mathrm{miss}}$) bins. The HT1-MET4 bin is excluded from the analysis, as explained in Section 5.6.

Observed number of events					
Sideband-fit SM background predictions					
$N_{\mathrm{b-jet}} \geq 3$	HT1	HT2	HT3	HT4	HT1-4
MET2	$119\,^{+32}_{-19}$	$158\,^{+36}_{-24}$	$28.2\,^{+6.9}_{-5.7}$	$10.2\,^{+3.5}_{-2.7}$	$316\,^{+49}_{-37}$
MET3	$15.2\,^{+4.3}_{-3.5}$	$27.7\,^{+5.8}_{-4.9}$	$5.6\,^{+2.6}_{-1.9}$	$2.0\,^{+1.5}_{-0.9}$	$50.5\,^{+8.2}_{-7.3}$
MET4	—	$8.3\,^{+2.9}_{-2.2}$	$1.9\,^{+1.3}_{-0.8}$	$0.4\,^{+0.6}_{-0.2}$	$10.5\,^{+3.2}_{-2.5}$
MET2-4	$134\,^{+32}_{-20}$	$194\,^{+36}_{-26}$	$35.7\,^{+7.5}_{-6.3}$	$12.6\,^{+3.8}_{-3.0}$	$377\,^{+51}_{-42}$

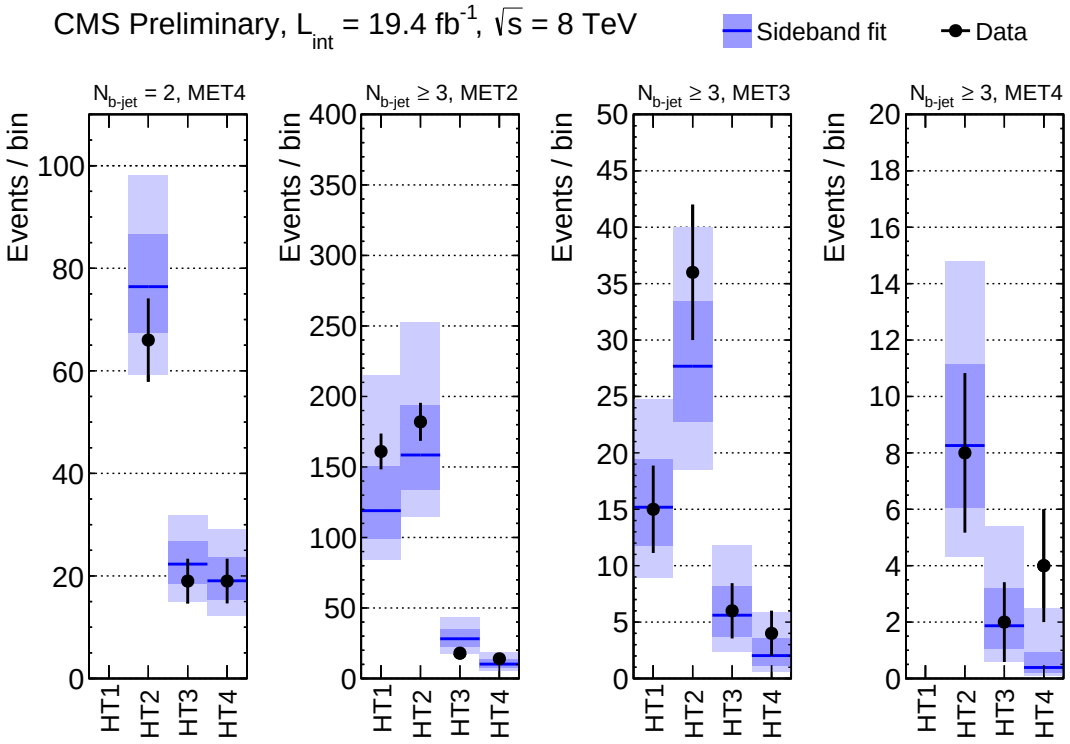

Figure 8: Observed number of events (points with error bars) for the 14 bins with highest signal sensitivity in the analysis. The dark- and light-shaded bands indicate the ± 1 and ± 2 standard deviation intervals, respectively, for the SM background estimates from the sideband fit.